



Insight into the structural requirements of proton pump inhibitors based on CoMFA and CoMSIA studies

M. Ravi Shashi Nayana, Y. Nataraja Sekhar, Haritha Nandyala, Ravikumar Muttineni*, Santosh Kumar Bairy, Kriti Singh, S.K. Mahmood

GVK Biosciences, Balanagar, Hyderabad, 500037 India

ARTICLE INFO

Article history:

Received 17 January 2008

Received in revised form 15 April 2008

Accepted 24 April 2008

Available online 9 May 2008

Keywords:

3D-QSAR

CoMFA

CoMSIA

Gastric (H⁺/K⁺)-ATPase

Proton pump inhibitors

ABSTRACT

In the present study, a series of 179 quinoline and quinazoline heterocyclic analogues exhibiting inhibitory activity against Gastric (H⁺/K⁺)-ATPase were investigated using the comparative molecular field analysis (CoMFA) and comparative molecular similarity indices (CoMSIA) methods. Both the models exhibited good correlation between the calculated 3D-QSAR fields and the observed biological activity for the respective training set compounds. The most optimal CoMFA and CoMSIA models yielded significant leave-one-out cross-validation coefficient, q^2 of 0.777, 0.744 and conventional cross-validation coefficient, r^2 of 0.927, 0.914 respectively. The predictive ability of generated models was tested on a set of 52 compounds having broad range of activity. CoMFA and CoMSIA yielded predicted activities for test set compounds with r^2_{pred} of 0.893 and 0.917 respectively. These validation tests not only revealed the robustness of the models but also demonstrated that for our models r^2_{pred} based on the mean activity of test set compounds can accurately estimate external predictivity. The factors affecting activity were analyzed carefully according to standard coefficient contour maps of steric, electrostatic, hydrophobic, acceptor and donor fields derived from the CoMFA and CoMSIA. These contour plots identified several key features which explain the wide range of activities. The results obtained from models offer important structural insight into designing novel peptic-ulcer inhibitors prior to their synthesis.

© 2008 Published by Elsevier Inc.

1. Introduction

The gastric (H⁺, K⁺)-ATPase belongs to a class of ion translocating ATPases that are characterized by the formation of a covalently phosphorylated enzyme intermediate as part of their catalytic cycle [1]. It is responsible for the final step of acid secretion in the stomach and is the main target in the pharmacological treatment of acid related diseases. Since their introduction into the market, irreversible inhibitors of the H⁺/K⁺-ATPase (proton pump inhibitors, PPIs) have revolutionized the treatment of gastro-oesophageal reflux disease (GERD) [2]. Despite of the clear success of these agents, there are still limitations of current GERD therapy with PPIs [3]. The final step of gastric acid secretion can be inhibited by agents that are competitive with respect to K⁺ binding to the parietal cell gastric (H⁺, K⁺)-ATPase [4–7]. These new reversible potassium competitive acid blockers (P-CABs) may offer therapeutic advantages over PPI therapy, and may have the potential to achieve faster inhibition of acid secretion and

longer duration of action compared to PPIs, resulting in quicker symptom relief and healing [8]. PPIs are further categorized into irreversible and reversible PPIs based on their blocking pattern [9].

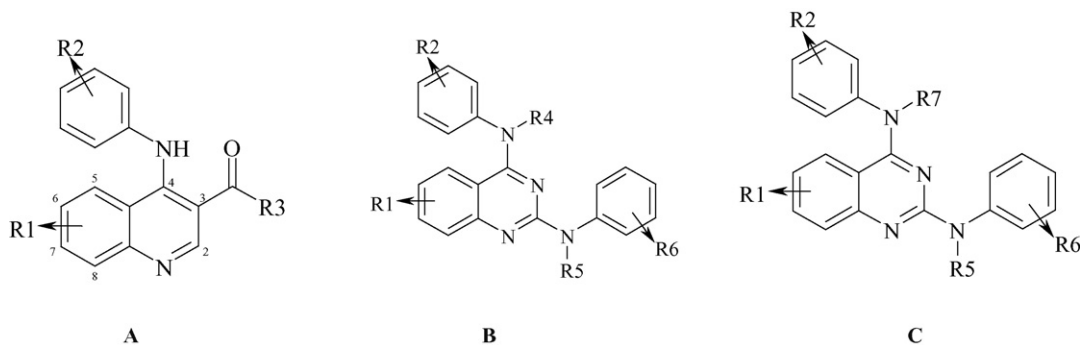
The reversible PPIs are categorized as potassium-competitive acid blockers (P-CABs) because they block the action of the (H⁺/K⁺)-ATPase by binding to or near the site of the K⁺ channel [10,11]. P-CAB binding to the proton pump is competitive and reversible, and these compounds inhibit acid secretion much more rapidly than do PPIs [12]. As a result, P-CABs can potentially be used for the treatment of GERD symptoms. The imidazopyridine based compound SCH28080 was the prototype of this class [13]. Agents in this class that are currently in development include CS-526 (R-105266; Sankyo/Novartis), soraprazan (BY359; Altana) and revaprazan (YH1885; Yuhan Pharmaceuticals).

Since drug discovery process is in the new direction involving various computational approaches including 3D-QSAR tools like CoMFA and CoMSIA, which have been increasingly employed in rational drug discovery process to understand the drug receptor interaction and to design new molecules. The main objective of the study is to report 3D-QSAR approach towards seeking insights into the structural requirements and binding affinities of gastric (H⁺/K⁺)-ATPase inhibitors. The essential information gathered by

* Corresponding author. Tel.: +91 4023721001.

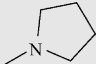
E-mail address: ravambio@gmail.com (R. Muttineni).

Table 1
Structures and activities of the molecules



Compound	Scaffold	R1	R2	R3	R4	R5	R6	R7	IC ₅₀ (μM)	pIC ₅₀
1	A	8-F	2-Me-4-OH	<i>n</i> -Pr	–	–	–	–	0.71	6.149
2	A	8-COOH	2-Me	<i>n</i> -Pr	–	–	–	–	5.90	5.229
3	A	8-COOMe	2-Me	<i>n</i> -Pr	–	–	–	–	0.58	6.236
4	A	8-CONH ₂	2-Me	<i>n</i> -Pr	–	–	–	–	1.90	5.721
5	A	8-Ac	2-Me	<i>n</i> -Pr	–	–	–	–	1.50	5.824
6	A	8-Ac	2-Me-4-OH	<i>n</i> -Pr	–	–	–	–	0.55	6.259
7	A	8-CH ₂ COOH	2-Me	<i>n</i> -Pr	–	–	–	–	7.20	5.142
8	A	8-CH ₂ COOEt	2-Me	<i>n</i> -Pr	–	–	–	–	18.4	4.735
9	A	8-CH ₂ OCONHMe	2-Me	<i>n</i> -Pr	–	–	–	–	6.60	5.18
10	A	8-NHCH ₂ CH ₂ OH	2-Me	<i>n</i> -Pr	–	–	–	–	7.10	5.149
11	A	8-O(CH ₂) ₃ COOEt	2-Me	<i>n</i> -Pr	–	–	–	–	1.60	5.796
12	A	8-1,3-dioxolan-4-yl	2-Me	<i>n</i> -Pr	–	–	–	–	36.0	4.444
13	A	8-O(CH ₂) ₃ NMe ₂	2-Me	<i>n</i> -Pr	–	–	–	–	0.39	6.409
14	A	8-O(CH ₂) ₂ NMe ₂	2-Me	<i>n</i> -Pr	–	–	–	–	0.51	6.284
15	A	8-O(CH ₂) ₃ -1-piperidino	2-Me	<i>n</i> -Pr	–	–	–	–	0.50	6.301
16	A	8-O(CH ₂) ₃ -1-morpholino	2-Me	<i>n</i> -Pr	–	–	–	–	0.89	6.051
17	A	8-O(CH ₂) ₃ -1-pyrrolidino	2-Me	<i>n</i> -Pr	–	–	–	–	0.51	6.292
18	A	8-O(CH ₂) ₃ N(Me)CH ₂ Ph	2-Me	<i>n</i> -Pr	–	–	–	–	0.65	6.187
19	A	8-O(CH ₂) ₃ N(Me)(CH ₂) ₃ Ph	2-Me	<i>n</i> -Pr	–	–	–	–	0.74	6.131
20	A	8-NH(CH ₂) ₃ -1-morpholino	2-Me	<i>n</i> -Pr	–	–	–	–	2.40	5.619
21	A	8-CH ₂ (2-imidazo[4,5- <i>c</i>]pyridyl)	2-Me	<i>n</i> -Pr	–	–	–	–	2.80	5.553
22	A	8-O(CH ₂) ₃ CONH(4-pyridyl)	2-Me	<i>n</i> -Pr	–	–	–	–	2.60	5.586
23	A	8-O-2-pyrazinyl	2-Me	<i>n</i> -Pr	–	–	–	–	2	5.699
24	A	8-O(6-Cl-4-pyridyl)	2-Me	<i>n</i> -Pr	–	–	–	–	6.90	5.161
25	A	8-O(2-pyridyl)	2,6-di-Me	Et	–	–	–	–	4.70	5.328
26	A	8-NH ₂	2,6-di-Me	<i>n</i> -Pr	–	–	–	–	5.80	5.236
27	A	8-O(CH ₂) ₃ NH(2-thiazolyl)	2,6-di-Me	Et	–	–	–	–	1.70	5.77
28	A	8-O(CH ₂) ₃ NH(2-pyridyl)	2,6-di-Me	<i>n</i> -Pr	–	–	–	–	0.90	6.046
29	A	8-O(CH ₂) ₃ (2-benzimidazolyl)	2,6-di-Me	<i>n</i> -Pr	–	–	–	–	1.40	5.854
30	A	8-O(CH ₂) ₃ (4-imidazolyl)	2,6-di-Me	<i>n</i> -Pr	–	–	–	–	0.60	6.222
31	A	8-O(CH ₂) ₃ NHAc	2,6-di-Me	<i>n</i> -Pr	–	–	–	–	1.80	5.745
32	A	8-O(CH ₂) ₃ CONH ₂	2,6-di-Me	<i>n</i> -Pr	–	–	–	–	2.20	5.657
33	A	8-O(CH ₂) ₃ CONHC(Me) ₂ CH ₂ OH	2,6-di-Me	<i>n</i> -Pr	–	–	–	–	2.80	5.552
34	A	6-OH	2-Me	<i>n</i> -Pr	–	–	–	–	0.24	6.619
35	A	6-OH	2-Me,4-OH	<i>n</i> -Pr	–	–	–	–	0.07	7.155
36	A	7-OH	2-Me	<i>n</i> -Pr	–	–	–	–	1.20	5.92
37	A	8-OH	2-Me	<i>n</i> -Pr	–	–	–	–	3.30	5.481
38	A	8-OH	2-Me-4-F	<i>n</i> -Pr	–	–	–	–	7.60	5.12
39	A	8-OH	2-Me	<i>i</i> -Pr	–	–	–	–	1.20	5.921
40	A	8-OH	2-Me-4-F	<i>i</i> -Pr	–	–	–	–	2.70	5.569
41	A	8-OH	2-Me	Et	–	–	–	–	0.86	6.065
42	A	8-OH	2-Me-4-F	Et	–	–	–	–	1.90	5.721
43	A	8-OCH ₂ CH ₂ OH	2-Me	Et	–	–	–	–	0.76	6.119
44	A	8-OCH ₂ CH ₂ OH	2-Me-4-F	Et	–	–	–	–	2	5.699
45	A	8-OCH ₂ CH ₂ OH	2-Me-4-F	<i>n</i> -Pr	–	–	–	–	2.70	5.569
46	A	8-OCH ₂ CH ₂ OH	2-Me-4-OH	<i>n</i> -Pr	–	–	–	–	0.21	6.678
47	A	8-OCH ₂ CH ₂ OH	2-Me	<i>i</i> -Pr	–	–	–	–	0.99	6.005
48	A	8-OCH ₂ CH ₂ OH	2-Me-4-F	<i>i</i> -Pr	–	–	–	–	1.60	5.796
49	A	8-OCH ₂ CH ₂ OMe	2-Me	Et	–	–	–	–	0.78	6.108
50	A	8-OCH ₂ CH ₂ OMe	2-Me-4-F	Et	–	–	–	–	2	5.699
51	A	8-OCH ₂ CH ₂ OMe	2-Me	<i>n</i> -Pr	–	–	–	–	2.50	5.602
52	A	8-OCH ₂ CH ₂ OMe	2-Me-4-F	<i>n</i> -Pr	–	–	–	–	3.50	5.456
53	A	8-OCH ₂ CH ₂ OMe	2-Me	<i>i</i> -Pr	–	–	–	–	1.40	5.854
54	A	8-OCH ₂ CH ₂ OMe	2-Me-4-F	<i>i</i> -Pr	–	–	–	–	1.70	5.77
55	A	8-(OCH ₂ CH ₂) ₂ OH	2-Me	<i>n</i> -Pr	–	–	–	–	2.10	5.677
56	A	8-(OCH ₂ CH ₂) ₂ OH	2-Me-4-F	<i>n</i> -Pr	–	–	–	–	4	5.398
57	A	8-(OCH ₂ CH ₂) ₃ OH	2-Me	<i>n</i> -Pr	–	–	–	–	2.40	5.62
58	A	8-(OCH ₂ CH ₂) ₃ OH	2-Me-4-F	<i>n</i> -Pr	–	–	–	–	3.60	5.444

Table 1 (Continued)

Compound	Scaffold	R1	R2	R3	R4	R5	R6	R7	IC ₅₀ (μM)	pIC ₅₀
59	A	8-O(CH ₂) ₃ OH	2,6-di-Me	<i>n</i> -Pr	–	–	–	–	1.21	5.917
60	A	6-CH ₂ OH	2-Me	<i>n</i> -Pr	–	–	–	–	4.40	5.356
61	A	8-CH ₂ OH	2-Me	Et	–	–	–	–	0.38	6.42
62	A	8-CH ₂ OH	2-Me-4-OH	Et	–	–	–	–	0.18	6.745
63	A	8-CH ₂ OH	2-Me	<i>n</i> -Pr	–	–	–	–	0.84	6.076
64	A	8-CH ₂ OH	2-Me-4-F	<i>n</i> -Pr	–	–	–	–	2.20	5.657
65	A	8-CH ₂ OH	2-Me-4-OH	<i>n</i> -Pr	–	–	–	–	6.18	5.209
66	A	8-CH ₂ OH	2-Me	<i>i</i> -Pr	–	–	–	–	0.84	6.086
67	A	8-CH ₂ OH	2-Me-4-F	<i>i</i> -Pr	–	–	–	–	2.10	5.678
68	A	8-CHO	2-Me	<i>n</i> -Pr	–	–	–	–	1.20	5.92
69	A	8-oxiranyl	2-Me	<i>n</i> -Pr	–	–	–	–	3	5.523
70	A	8-CH(OH)CH=CH ₂	2-Me	<i>n</i> -Pr	–	–	–	–	0.66	6.18
71	A	8-CH(OH)Me	2-Me	<i>n</i> -Pr	–	–	–	–	0.37	6.431
72	A	8-CH(OH)Me	2-Me-4-OH	<i>n</i> -Pr	–	–	–	–	0.061	7.215
73	A	8-CH=CHCH ₂ OH	2-Me	<i>n</i> -Pr	–	–	–	–	2.30	5.638
74	A	8-2-(hydroxymethyl)oxiranyl	2-Me	<i>n</i> -Pr	–	–	–	–	3.10	5.508
75	A	8-2-(hydroxymethyl)oxiranyl	2-Me	<i>n</i> -Pr	–	–	–	–	3.10	5.508
76	A	8-OMe	2-Me	<i>n</i> -Pr	–	–	–	–	1.70	5.77
77	A	8-OMe	H	<i>n</i> -Pr	–	–	–	–	4	5.397
78	A	8-OMe	2,3-di-Me	<i>n</i> -Pr	–	–	–	–	1.40	5.854
79	A	8-OMe	2,4-di-Me	<i>n</i> -Pr	–	–	–	–	4.30	5.366
80	A	8-OMe	2,5-di-Me	<i>n</i> -Pr	–	–	–	–	2.50	5.602
81	A	8-OMe	2,6-di-Me	<i>n</i> -Pr	–	–	–	–	1.60	5.796
82	A	8-OMe	2,4,6-tri-Me	<i>n</i> -Pr	–	–	–	–	3.10	5.508
83	A	8-OMe	3,5-di-Me	<i>n</i> -Pr	–	–	–	–	11.3	4.947
84	A	8-OMe	2-Me	<i>n</i> -Pr	–	–	–	–	1.69	5.77
85	A	8-OCH ₂ CH ₂ OH	2-Me	<i>n</i> -Pr	–	–	–	–	2	5.619
86	A	8-OMe	2-Et	<i>n</i> -Pr	–	–	–	–	0.88	6.051
87	A	8-OMe	2-OEt	<i>n</i> -Pr	–	–	–	–	1.99	5.699
88	A	8-OMe	2-OMe	<i>n</i> -Pr	–	–	–	–	1.50	5.824
89	A	8-OMe	2,4-di-OMe	<i>n</i> -Pr	–	–	–	–	2.10	5.678
90	A	8-OMe	2,4,6-tri-OMe	<i>n</i> -Pr	–	–	–	–	4.60	5.337
91	A	8-OMe	2-Me-4-OMe	<i>n</i> -Pr	–	–	–	–	1.27	5.896
92	A	8-OMe	2-CH ₂ OH	<i>n</i> -Pr	–	–	–	–	12	4.921
93	A	8-OMe	2-CH ₂ OMe	<i>n</i> -Pr	–	–	–	–	5.50	5.259
94	A	8-OMe	2-Me-3-CH ₂ OH	<i>n</i> -Pr	–	–	–	–	6	5.222
95	A	8-OMe	2-Me-5-CH ₂ OH	<i>n</i> -Pr	–	–	–	–	10.2	4.991
96	A	8-OMe	2-OH	<i>n</i> -Pr	–	–	–	–	1.30	5.886
97	A	8-OMe	4-OH	<i>n</i> -Pr	–	–	–	–	0.67	6.174
98	A	8-OMe	2-Me-4-OH	<i>n</i> -Pr	–	–	–	–	0.21	6.677
99	A	8-OMe	2,6-di-Me-4-OH	<i>n</i> -Pr	–	–	–	–	0.50	6.301
100	A	8-OMe	2-Me-4-(OCOEt)	<i>n</i> -Pr	–	–	–	–	19	4.721
101	A	8-OMe	2,6-di-Me-3,4-di-OH	<i>n</i> -Pr	–	–	–	–	2.80	5.553
102	A	8-OMe	3,4-Methylenedioxy	<i>n</i> -Pr	–	–	–	–	3.60	5.443
103	A	8-OMe	2,6-di-Me-3,4-methylenedioxy	<i>n</i> -Pr	–	–	–	–	2.70	5.568
104	A	8-OMe	2-Me-4-O(CH ₂) ₃ -3-imidazolyl	<i>n</i> -Pr	–	–	–	–	34	4.468
105	A	8-OMe	2-Me-4-F	<i>n</i> -Pr	–	–	–	–	2.30	5.639
106	A	8-OMe	2-Me-4-NH ₂	<i>n</i> -Pr	–	–	–	–	1.50	5.823
107	A	8-OMe	2-Me-4-NMe ₂	<i>n</i> -Pr	–	–	–	–	2.32	5.634
108	A	8-OMe	2-Me-4-NHAc	<i>n</i> -Pr	–	–	–	–	12	4.921
109	A	8-OMe	2-Me-4-NHSO ₂ Me	<i>n</i> -Pr	–	–	–	–	45	4.347
110	A	8-Me	H	<i>n</i> -Pr	–	–	–	–	3	5.523
111	A	8-Me	2-Me	<i>n</i> -Pr	–	–	–	–	2.99	5.523
112	A	8-Me	6-Me	<i>n</i> -Pr	–	–	–	–	3.10	5.509
113	A	8-Me	2,6-di-Me	<i>n</i> -Pr	–	–	–	–	3.10	5.508
114	A	8-Me	2-Et	<i>n</i> -Pr	–	–	–	–	2.90	5.537
115	A	8-Me	2-OMe	<i>n</i> -Pr	–	–	–	–	2.20	5.657
116	A	8-Me	2,4-di-OMe	<i>n</i> -Pr	–	–	–	–	2.40	5.62
117	A	8-Me	2-Me-4-OMe	<i>n</i> -Pr	–	–	–	–	1.70	5.77
118	A	8-Me	2-Cl	<i>n</i> -Pr	–	–	–	–	6.30	5.201
119	A	H	2-Me	<i>n</i> -Pr	–	–	–	–	0.97	6.013
120	A	H	2-Me	<i>n</i> -Pr	–	–	–	–	0.96	6.014
121	A	2-Me	2-Me	<i>n</i> -Pr	–	–	–	–	34	4.468
122	A	6-OMe	2-Me	<i>n</i> -Pr	–	–	–	–	7	5.155
123	A	6-NH ₂	2,6-di-Me	<i>n</i> -Pr	–	–	–	–	0.16	6.796
124	A	6-OH-8-OMe	2-Me	<i>n</i> -Pr	–	–	–	–	1.30	5.886
125	A	6-OH-8-OMe	2-Me-4-F	<i>n</i> -Pr	–	–	–	–	2.10	5.677
126	A	8-NH ₂	2-Me	<i>n</i> -Pr	–	–	–	–	3	5.222
127	B	8-Me	2-Me	–	NH ₂	–	–	–	0.23	6.62
128	B	8-OMe	2-Me	–	NH ₂	–	–	–	0.08	7.097
129	B	8-OMe	2-Me	–	NHCH ₃	–	–	–	0.641	6.193
130	B	8-OMe	2-Me	–	N(CH ₃) ₂	–	–	–	15.9	4.796
131	B	8-OMe	2-Me	–		–	–	–	30	4.522

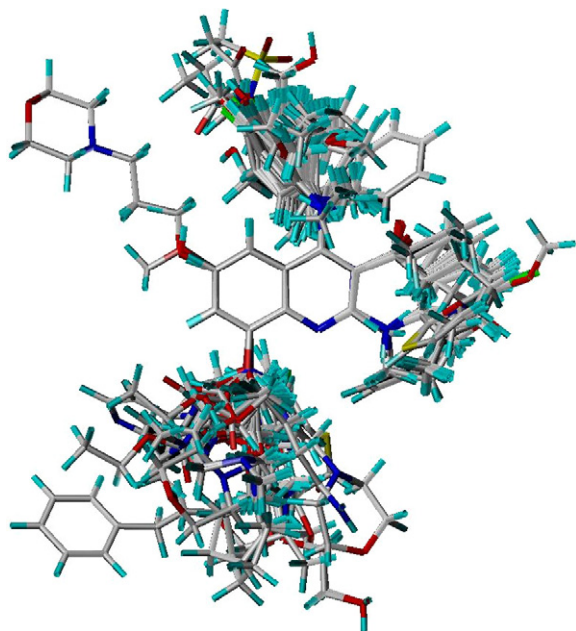


Fig. 1. 3D-view of aligned molecules (training and test sets) based on rms fit alignment method.

performing 3D-QSAR could be helpful to understand the structure activity relationships of the series undertaken and subsequently for the design of new potent inhibitors.

2. Materials and methods

2.1. Dataset and molecular modeling

A dataset of 179 quinoline and quinazoline heterocyclic analogues reported to have gastric (H^+/K^+)-ATPase inhibitory activities [14,15] were used for the following QSAR studies (Table 1). *In vitro* inhibitory concentrations (IC_{50}) of the molecules against gastric (H^+/K^+)-ATPase were converted into corresponding pIC_{50} and used as dependent variables in the 3D-QSAR calculations. All the molecules were divided into training set (127 compounds) for generating 3D-QSAR models and a test set (52 compounds) for validating the quality of the models. The test set was selected based on the criteria given by Oprea et al. [16].

All molecular studies were performed using the molecular modeling package SYBYL 6.7.1 [17] on silicon graphics workstation. Energy minimization was performed in SYBYL using Tripos force field [18]. The conformations were generated for the most active compound **163**. As the compound is relatively rigid hence we have used systematic search method with a step size of 15° torsion angle to generate the conformational model. The lowest energy conformer was selected and further geometry optimization of each molecule was carried out with MOPAC 6 package using the semi-empirical AM1 Hamiltonian [19]. Optimized structures with MOPAC charges were used for subsequent calculations. This conformer was considered for the building of other molecules.

To extract the common features among the highly active compounds, we have generated a qualitative pharmacophore model using 23 compounds having activity >7.0 (pIC_{50}) with the help of Hip-Hop module of Catalyst software. Multiple acceptable conformations were generated for all ligands within the catalyst [20] ConForm module using the Poling algorithm [21]. A maximum of 250 conformations were generated for each molecule within an energy threshold of 20.0 kcal/mol above the global energy minimum.

2.2. Alignment procedure

In standard CoMFA procedure, bioactive conformations [22] are desired for superimposing ligands. In the absence of available crystallographic data information on gastric (H^+/K^+)-ATPase and inhibitor complexes, we assumed that the active conformer corresponds to the lowest energy conformer of the conformational model. The molecular alignment was carried out using the atom-based RMS fit method with ALIGN DATABASE command available in SYBYL. This option uses alignment of structures through pairwise atom super positioning, places all structures in the database in the same frame of reference as the template compound. The most active compound, **163** was used as template and the remaining molecules were aligned to it through using the basic core of quinoline. The aligned molecules are shown in Fig. 1.

2.3. CoMFA and CoMSIA

The CoMFA [23] steric and electrostatic interaction energy fields were generated using a sp^3 hybridized carbon atom as a probe with +1 point charge. The energy cut off for the steric and electrostatic interaction energies was set to 30 kcal/mol.

In CoMSIA [24,25], all five physicochemical descriptors (electrostatic, steric, hydrophobic, and H-bond donor and acceptor) were evaluated at each lattice interactions of a regularly spaced grid of 2.0 Å. A probe atom within radius of 1 Å, +1 charge, hydrophobicity +1.0, H-bond donor and acceptor properties of +1.0 was used to evaluate steric, electrostatic, hydrophobic, H-bond donor and acceptor fields. For attenuation factor α controlling the steepness of Gaussian function the standard value of 0.3 was accepted.

2.4. PLS analysis

In PLS analysis [26,27], the cross validation was performed using leave-one-out (LOO) method wherein one compound is removed from the dataset and its activity is predicted using the model derived from the rest of the dataset. The cross-validated q^2 that resulted in optimum number of components (ONC) was considered. To speed up the analysis and to reduce noise, a minimum default column-filtering value (σ) of 2.00 kcal/mol (CoMFA) and 1.00 kcal/mol (CoMSIA) was used so that only those descriptor energies with values greater than the above described will be considered for PLS analysis. Final analysis (non-cross-validated) was performed to calculate conventional r^2 using the optimum number components obtained from the leave-one-out cross-validation analysis. The predictive ability of the 3D-QSAR models was determined using formula:

$$r_{pred}^2 = \frac{(SD - PRESS)}{SD}$$

where SD is the sum of squared deviations between the biological activities of each molecule and the mean activity of the training set molecules and PRESS is the sum of squared deviations between the predicted and actual activity values for every molecule in the test set.

3. Results and discussion

3.1. CoMFA statistical details

The predictive 3D-QSAR models were generated for the training set of 127 gastric (H^+/K^+) ATPase inhibitors using default parameters of COMFA, as determined by cross validation. Reliability of the QSAR models was statistically validated using

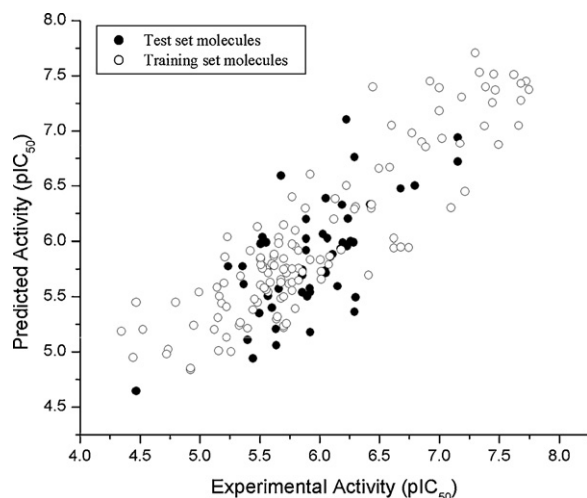


Fig. 2. Experimental activities versus predicted activities for compounds in the training and test sets using CoMFA model.

several statistical parameters, such as r^2 , q^2 and r^2_{pred} . The CoMFA models yielded a good cross-validated correlation coefficient with LOO of 0.777 and with leave-many-out (q^2 with 10 groups) was 0.751, thus the predictions obtained with these models were reliable. These internal validation methods (leave-one-out and leave-many-out) determine the stability of the developed models. The non-cross-validated PLS analysis gave a good correlation coefficient r^2 of 0.927 with a standard error of estimate (SEE) of 0.225. F -value stands for the degree of statistical confidence on the developed models and the model has good value of 253. The steric and electrostatic contributions are 48.4% and 51.6%, respectively. Fig. 2 shows the graph of actual versus predicted pIC_{50} values of the compounds using CoMFA model. The statistical data obtained from the standard CoMFA model constructed with steric and electrostatic fields are depicted in Table 2.

3.2. CoMSIA statistical details

CoMSIA, a newer 3D-QSAR technique, allows more incisive dissection of different binding affinity contributions, including the steric and electrostatic contributions as well as the entropic effects, which are harder to quantify and moreover it is touted to be less affected by changes in molecular alignment and to provide more smooth and interpretable contour maps as a result of employing

Table 2
Statistical parameters of the CoMFA and CoMSIA models

Parameter	CoMFA	CoMSIA
r^2	0.927	0.914
q^2	0.777	0.744
SEE	0.225	0.245
n	5	6
F -value	253	211.31
r^2_{pred}	0.893	0.917
Field contribution		
Steric	0.484	0.096
Electrostatic	0.516	0.252
Hydrophobic	–	0.190
Donor	–	0.205
Acceptor	–	0.257

r^2 , non-cross validated correlation coefficient; q^2 , LOO cross-validated correlation coefficient; SEE, standard error of estimate; n , number of components used in the PLS analysis; F -value, F -statistic for the analysis; r^2_{pred} , predictive correlation coefficient.

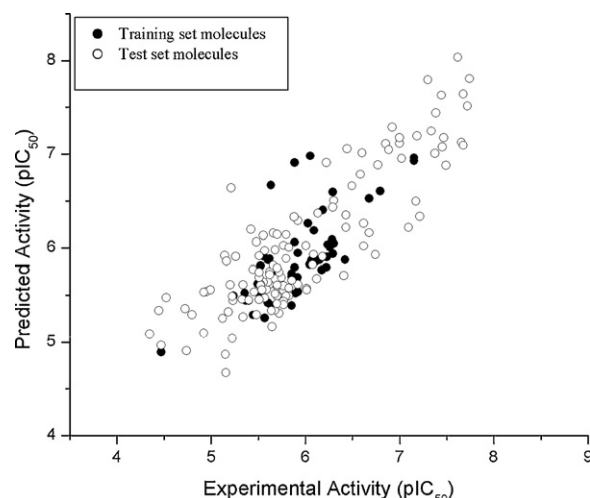


Fig. 3. Experimental activities versus predicted activities for compounds in the training and test sets using CoMSIA models.

Gaussian type distance dependence with the molecular similarity indices it uses [26]. A cross-validated correlation coefficient of 0.744 and 0.743 using LOO and with q^2 (10 groups) respectively was obtained when all the five descriptors were considered and six components were observed in both the models. The conventional correlation coefficient, r^2 of 0.914 between the actual and observed activities of the molecules was obtained with this model. The q^2 values of the CoMSIA model compared to the CoMFA model indicating stable analyses of high quality. Further the CoMSIA model comprise of valuable complementary information, as they offer comparative and additional explanation for ligands by introducing three auxiliary field types, the hydrophobic field, the H-bond donor and acceptor fields. The CoMSIA statistical details are given in Table 2. Fig. 3 shows the experimental activities versus predicted ones in the training and test sets by CoMSIA model. Final predicted versus experimental pIC_{50} values for both CoMFA and CoMSIA models and their residuals (for training and test set compounds) are given in Tables 3 and 4.

3.3. Validation of CoMFA and CoMSIA models

Tropsha has emphasized that high q^2 (>0.5) is a necessary but not sufficient condition for a predictive QSAR model. The best model should also predict the activities well, for the compounds which are not included in the training set. A test set of 52 compounds, having wide range of activities was considered for external prediction (r^2_{pred}). The test compounds are in good agreement with the observed activity within a tolerable error range and substantiated by the r^2_{pred} value of 0.893 and 0.917 for CoMFA and CoMSIA, respectively. Figs. 2 and 3 show that both the CoMFA and CoMSIA models are reliable and can be useful in designing new potent gastric (H^+/K^+)-ATPase inhibitors.

3.4. Interpretation of contour maps

The contour maps obtained by CoMFA and CoMSIA show how 3D-QSAR methods can identify features important for the interaction between ligands and the target protein. They allow identification of those positions that require a particular physicochemical property to enhance the bioactivity of a ligand. Figs. 4 and 5 indicate CoMFA and Figs. 6 and 7 indicate CoMSIA steric and electrostatic contour maps, respectively. In Figs. 4 and 6, the green contours represent regions of high steric tolerance (80%

Table 3
Activities and residuals of training set for CoMFA and CoMSIA models

Compound	Exp. activity	CoMFA		CoMSIA	
		Predicted	Residual	Predicted	Residual
2	5.229	6.036	−0.807	5.443	−0.214
4	5.721	5.755	−0.034	5.442	0.279
5	5.824	5.756	0.068	5.493	0.331
7	5.142	5.583	−0.441	5.921	−0.778
8	4.735	5.022	−0.287	4.91	−0.174
9	5.18	5.442	−0.262	5.322	−0.142
10	5.149	5.31	−0.161	4.87	0.279
11	5.796	5.955	−0.159	5.889	−0.093
12	4.444	4.951	−0.507	5.338	−0.895
13	6.409	5.694	0.715	5.711	0.698
14	6.301	6.311	−0.01	6.503	−0.202
17	6.292	6.29	0.002	6.43	−0.138
19	6.131	6.382	−0.251	6.367	−0.236
20	5.619	5.862	−0.243	5.615	0.005
22	5.586	5.629	−0.043	5.56	0.025
23	5.699	5.217	0.482	5.593	0.106
24	5.161	5.504	−0.343	5.862	−0.701
25	5.328	5.241	0.087	5.457	−0.129
27	5.77	5.973	−0.203	5.554	0.215
31	5.745	5.616	0.129	5.687	0.057
32	5.657	6.031	−0.374	6.155	−0.497
33	5.552	5.757	−0.205	6.131	−0.578
34	6.619	5.942	0.677	6.26	0.359
37	5.481	5.45	0.031	5.293	0.189
38	5.12	5.202	−0.082	5.253	−0.133
40	5.569	5.545	0.024	5.47	0.098
41	5.721	5.713	0.008	5.307	0.414
43	6.119	6.199	−0.08	5.677	0.442
44	5.699	6.145	−0.446	6.141	−0.442
45	5.569	5.715	−0.146	5.972	−0.404
46	6.678	5.948	0.73	6.159	0.519
47	6.005	5.833	0.172	6.022	−0.017
48	5.796	6.097	−0.301	6.14	−0.344
50	5.699	5.845	−0.146	5.493	0.206
51	5.602	5.799	−0.197	5.641	−0.039
52	5.456	5.478	−0.022	5.535	−0.080
54	5.77	5.63	0.14	5.602	0.167
55	5.677	5.484	0.193	5.341	0.336
56	5.398	5.214	0.184	5.448	−0.05
57	5.62	5.884	−0.264	5.748	−0.128
58	5.444	5.382	0.062	5.772	−0.329
62	6.745	5.945	0.800	5.93	0.815
63	6.076	5.791	0.285	5.825	0.250
64	5.209	5.858	−0.649	6.636	−0.427
65	6.086	5.865	0.221	5.933	0.154
67	5.678	5.656	0.022	5.979	−0.301
68	5.92	5.834	0.086	5.618	0.303
70	6.18	5.926	0.254	5.909	0.271
71	6.431	6.295	0.136	6.215	0.217
72	7.215	6.447	0.768	6.335	0.88
74	5.508	5.838	−0.33	5.918	−0.41
76	5.77	6.4	−0.63	6.026	−0.256
81	5.796	5.393	0.403	5.495	0.301
82	5.508	5.604	−0.096	5.455	0.054
83	4.947	5.242	−0.295	5.538	−0.591
84	5.77	5.555	0.215	5.435	0.334
85	5.699	5.75	−0.051	5.609	0.09
88	5.824	5.648	0.176	5.578	0.246
89	5.678	5.628	0.05	5.515	0.162
90	5.337	5.265	0.072	5.267	0.07
92	4.921	4.839	0.082	5.094	−0.173
93	5.259	5.003	0.256	5.911	−0.652
94	5.222	5.409	−0.187	5.49	−0.268
95	4.991	5.542	−0.551	5.558	−0.567
100	4.721	4.981	−0.26	5.357	−0.636
101	5.553	5.563	−0.01	5.639	−0.086
105	5.639	5.295	0.344	5.335	0.303
106	5.823	5.918	−0.095	6.007	−0.183
108	4.921	4.854	0.067	5.532	−0.611
109	4.347	5.189	−0.842	5.084	−0.737
110	5.523	5.777	−0.254	5.616	−0.093
111	5.523	5.756	−0.233	5.605	−0.082
112	5.509	5.789	−0.28	5.691	−0.182

Table 3 (Continued)

Compound	Exp. activity	CoMFA		CoMSIA	
		Predicted	Residual	Predicted	Residual
113	5.508	5.853	−0.345	5.744	−0.235
114	5.537	5.581	−0.044	5.556	−0.019
115	5.657	5.981	−0.324	5.817	−0.159
116	5.62	5.782	−0.162	5.718	−0.098
117	5.77	5.752	0.018	5.4	0.37
118	5.201	5.624	−0.423	5.61	−0.409
119	6.013	5.728	0.285	5.574	0.44
120	6.014	5.658	0.356	5.559	0.454
121	4.468	5.45	−0.982	4.966	−0.497
125	5.155	5.012	0.143	4.673	0.482
126	5.222	5.132	0.09	5.04	0.182
127	6.62	6.026	0.594	6.021	0.599
128	7.097	6.302	0.795	6.214	0.883
130	4.796	5.45	−0.654	5.292	−0.496
131	4.522	5.205	−0.683	5.475	−0.952
132	5.698	5.234	0.464	5.41	0.289
134	5.721	5.256	0.465	5.743	−0.022
135	5.42	5.917	−0.497	6.195	−0.775
136	5.481	6.13	−0.649	6.062	−0.581
137	5.92	6.603	−0.683	6.29	−0.369
139	6.222	6.503	−0.281	6.911	−0.689
141	5.699	5.5	0.199	5.789	−0.09
143	7.174	6.884	0.29	6.497	0.677
145	7.187	7.307	−0.12	7.195	−0.007
146	7.658	7.049	0.609	7.125	0.532
147	7.377	7.044	0.333	7.005	0.371
148	6.495	6.656	−0.161	6.661	−0.166
149	7.721	7.45	0.271	7.515	0.206
150	7.337	7.53	−0.193	7.246	0.091
151	7.468	7.369	0.099	7.173	0.295
152	6.921	7.45	−0.529	7.288	−0.367
153	7	7.181	−0.181	7.112	−0.112
154	7.022	6.932	0.09	6.954	0.068
155	5.88	6.296	−0.416	6.328	−0.449
156	7.678	7.276	0.402	7.093	0.585
157	7.495	6.875	0.62	6.88	0.614
158	7.387	7.4	−0.013	7.44	−0.053
159	6.444	7.398	−0.954	7.056	−0.612
161	6.602	7.051	−0.449	7.013	−0.411
162	7.62	7.508	0.112	8.034	−0.414
163	7.745	7.375	0.37	7.805	−0.06
165	5.857	5.725	0.132	5.658	0.199
166	6.432	6.331	0.101	6.349	0.082
167	6.853	6.901	−0.048	7.11	−0.256
168	6.586	6.668	−0.082	6.784	−0.199
169	6.77	6.982	−0.212	6.884	−0.115
170	7.456	7.513	−0.057	7.075	0.381
171	7	7.392	−0.392	7.174	−0.174
172	6.886	6.854	0.032	7.045	−0.159
173	7.678	7.429	0.249	7.641	0.037
174	7.444	7.255	0.189	7.628	−0.184
175	7.301	7.706	−0.405	7.794	−0.493
176	5.646	5.319	0.327	5.164	0.482
179	5.338	5.686	−0.348	5.611	−0.274

contribution), while the yellow contours represent regions of low steric bulk tolerance (20% contribution). In Figs. 5 and 7, the increase in positive charge is favored in blue regions while increase in negative charge is favored in red regions.

3.5. CoMFA analysis

3.5.1. Steric analysis

Fig. 4 shows sterically favored (green) and disfavored (yellow) regions mapped on the highest active compound **163**, obtained from CoMFA analysis. The green contour mapped towards the right lower region of the C⁸ position of heterocyclic ring, suggests that the longer carbon-linker chain substituents towards this spatial distribution increase the activity. The compounds **173**, **174**, and **175** are showing higher activity as the substituents of these

Table 4

Activities and residuals of test set for CoMFA and CoMSIA models

Compound	Exp. activity	CoMFA		CoMSIA	
		Predicted	Residual	Predicted	Residual
1	6.149	5.595	0.554	5.876	0.273
3	6.236	6.203	0.033	6.036	0.2
6	6.259	5.998	0.261	6.009	0.25
15	6.284	5.989	0.295	6.088	0.196
16	6.051	6.388	−0.337	6.979	−0.928
18	6.187	6.328	−0.141	6.402	−0.215
21	5.553	5.991	−0.438	5.916	−0.363
26	5.236	5.775	−0.539	5.492	−0.256
28	6.046	5.735	0.311	5.826	0.22
29	5.854	5.744	0.11	5.7	0.154
30	6.222	7.104	−0.882	5.796	0.426
35	7.155	6.939	0.216	6.96	0.195
36	5.92	5.542	0.378	5.948	−0.028
39	5.921	5.179	0.742	5.539	0.382
42	6.065	6.028	0.037	5.871	0.194
49	6.108	5.885	0.223	5.854	0.254
53	5.854	5.541	0.313	5.39	0.464
59	5.917	5.576	0.341	5.69	0.227
60	5.356	5.775	−0.419	5.523	−0.167
61	6.42	6.332	0.088	5.877	0.543
66	5.657	5.571	0.086	5.79	−0.133
69	5.523	6.037	−0.514	5.814	−0.291
73	5.638	5.06	0.578	5.39	0.248
75	5.508	5.978	−0.47	5.522	−0.014
77	5.397	5.109	0.288	5.444	−0.047
78	5.854	5.693	0.161	5.73	0.124
79	5.366	5.613	−0.247	5.442	−0.076
80	5.602	5.399	0.203	5.421	0.181
86	5.619	5.781	−0.162	5.889	−0.27
87	6.051	5.716	0.335	5.835	0.216
91	5.896	5.503	0.393	5.521	0.375
96	5.886	6.198	−0.312	6.909	−1.023
97	6.174	5.934	0.24	5.77	0.404
98	6.677	6.475	0.202	6.527	0.15
99	6.301	5.495	0.806	6.049	0.252
102	5.443	4.941	0.502	5.289	0.154
103	5.568	5.507	0.061	5.257	0.311
104	4.468	4.646	−0.178	4.895	−0.427
107	5.634	5.209	0.425	6.668	−1.034
123	6.796	6.503	0.293	6.605	0.191
124	5.886	5.919	−0.033	5.796	0.09
125	5.677	6.591	−0.914	5.763	−0.086
129	6.193	5.986	0.207	5.908	0.285
133	5.495	5.352	0.143	5.621	−0.126
138	6.027	6.064	−0.037	6.262	−0.235
140	5.602	5.784	−0.182	5.875	−0.273
142	6.229	5.956	0.273	5.907	0.322
144	7.154	6.718	0.436	6.929	0.225
160	6.292	6.76	−0.468	6.594	−0.302
164	5.886	6.023	−0.137	6.061	−0.175
177	6.292	5.365	0.927	5.942	0.35
178	6.091	5.863	0.228	6.184	−0.093

compounds are projected in green region. The yellow contour map shown towards the left lower region of this position indicates that the longer chain substituents towards this spatial distribution decrease the activity. In case of the compounds of scaffold A (compounds **8–12**), the bulkier substitutions are occupied in this region as seen in **8–10** and **12** and showing less activity. A big green contour is mapped over the substituted phenyl group positioned at C² of the heterocyclic ring. It indicates that a large hydrophobic pocket may be present in the receptors active site to accommodate the steric bulk in these regions and contributes for binding affinity. This may be one of the reasons for the compounds containing scaffold C are showing average to higher activity as they contain methyl-substituted phenyl ring at C² position. The steric contour of CoMFA (Fig. 4) shows a green contour along with two yellow contours little further away enclosing the C⁴ position of the

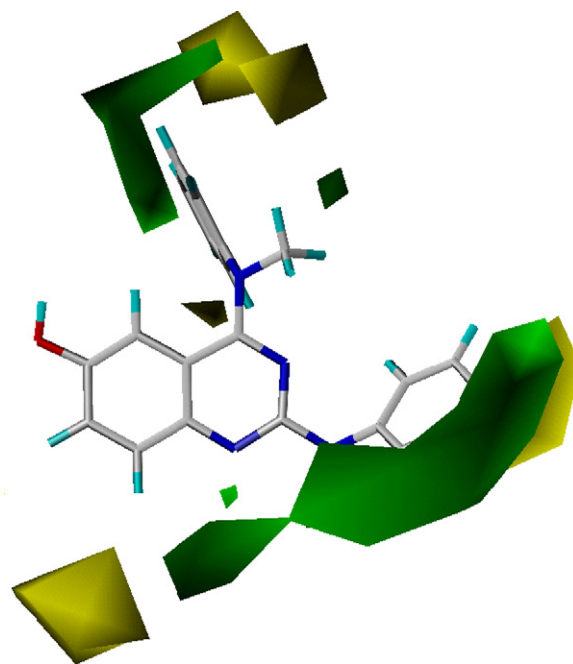


Fig. 4. CoMFA contour maps illustrating steric features in combination with compound **163**. The green contour for steric favored region and yellow maps calls for a reduction of this potential to improve affinity.

heterocyclic ring. This indicates that the moderately bulky substituents at the *ortho* and *para* positions of the phenyl ring improved activity as in **76**, **81**, **87**, **96–99**. The yellow blocks which are further away indicate that the larger bulky groups with longer chain substituents at the *meta* and *para* positions decrease the activity, as in **100**, **104**, and **109**.

3.5.2. Electrostatic analysis

The electrostatic contour maps obtained from CoMFA analysis were mapped on to the compound **163** were shown in the Fig. 5. The presence of red contour map at the C⁸ position of the heterocyclic scaffold indicates that the substituents having electronegative group attached at this position show improved

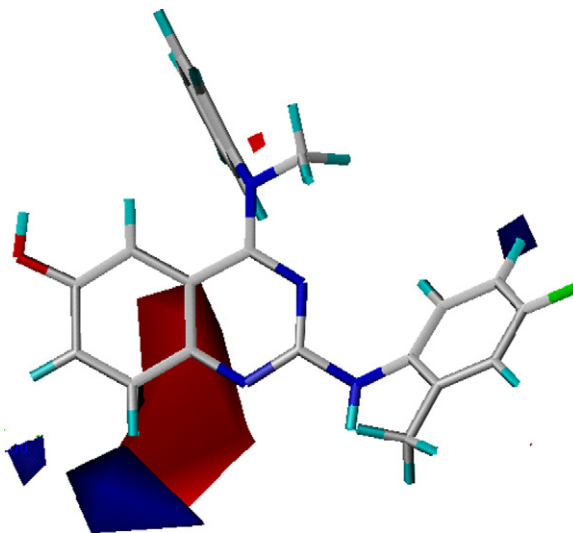


Fig. 5. CoMFA contour maps illustrating electrostatic features in combination with compound **163**. The red contour for negative charge favored region; blue for positive charge preferred region to improve binding affinity.

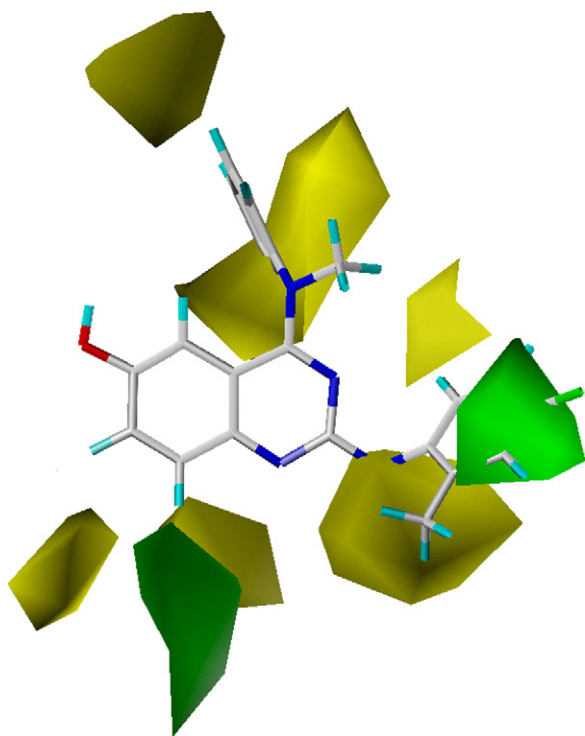


Fig. 6. CoMSIA contour maps illustrating steric features in combination with compound **163**. The green contour for steric favored region and yellow maps calls for a reduction of this potential to improve affinity.

activity as observed in the **76**, **81**, **86**, and **88** against the unsubstituted compounds **110**, **113**, **114**, and **115** respectively. The compounds **172** and **174** are showing higher activity as their electropositive substituents at this position are mapped to the green contour appeared at this position.

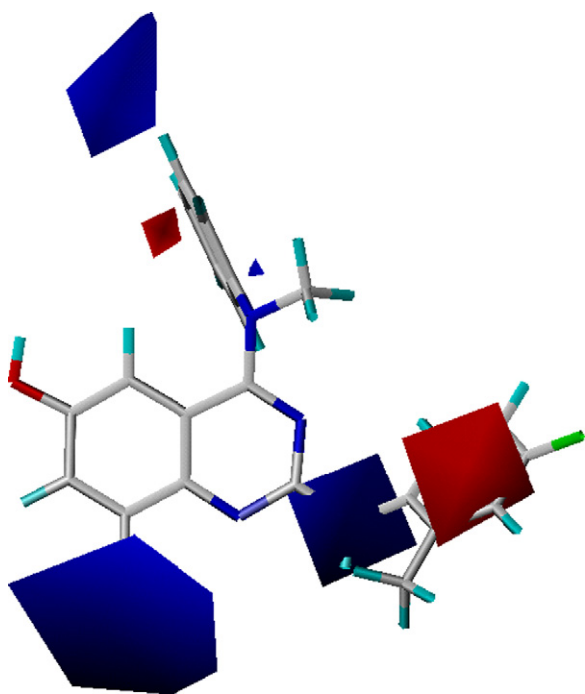


Fig. 7. CoMSIA contour maps illustrating electrostatic features in combination with compound **163**. The red contour for negative charge favored region; blue for positive charge preferred region to improve binding affinity.

3.6. CoMSIA analysis

3.6.1. Steric contour analysis

Fig. 6 shows sterically favored (green) and disfavored (yellow) regions. The green contour mapped near the C⁸ position of heterocyclic ring, suggests that bulkier groups are favored at this position. The compound **73** is showing higher activity as the substituents of this compound is projected in green region. The yellow contour map shown towards the left lower region of this position indicates that the longer chain substituents towards this spatial distribution decrease the activity. The contour at this position is also observed in CoMFA map (**Fig. 4**). The green contour which is mapped over the phenyl group positioned at C² of the heterocyclic ring shows the steric bulk in these regions is favored (similar contour map was also appeared in CoMFA). The yellow contour at C² signifies that the steric substituents at R5 position are disfavored (in case of compounds **121**, **130**, **141**). Yellow blocks appeared at 4th and 5th positions of phenyl ring indicate that the bulky groups with longer chain substituents decrease the activity. The compounds **83**, **95**, **100**, **104**, **108** and **109** are having less activity as they are overlapping on these blocks.

3.6.2. Electrostatic contour analysis

The electrostatic contour maps shown by the CoMSIA model (**Fig. 7**) are more informative than that of CoMFA model (**Fig. 5**), as they give more detailed picture in the case of R2 and R4 and R6 substitutions. The large blue contour map positioned near C⁸ of heterocyclic ring illustrates that electropositive groups are favored at this position. This favorable electropositive contour is also observed in the CoMFA model (**Fig. 5**).

As depicted from the **Fig. 7**, blue contour map of CoMSIA model shown at the lower corner further away from the red contour map at the 8th position of the heterocyclic ring denotes that electropositive groups are favored at this region. As it also favors steric groups at this position (**Fig. 6**), the longer carbon linker chains having substituted amino group shows increased activity as noted in compounds **13–19** and **173–175**. The blue contour map noted adjacent to the 2nd position of the heterocyclic ring indicates the electropositive substitutions are favored at this region. The compound **128** is having higher activity due to the presence of amine group at this position. Activity decreased with electropositive character as in case of the compounds **128**, **129**, and **130**. This might be one of the reasons for compounds with scaffold C, having substituted amine group at this position, showing moderate to higher activity. The red contour map observed at distal region away from blue contour of 2nd position specifies the region for electronegative groups. The electronegative substituted phenyl ring was buried inside this red contour as shown in the highest active compound **163** (**Fig. 7**). It was also absorbed in other compounds having phenyl ring with substituted with halogens are showing higher activity (**156**, **156**, **157**, **158**, **161**, and **163**). The compound **162** with electropositive substituted phenyl ring at this position is showing decreased activity. The appearance of blue contour near C⁴ position of phenyl ring, favor electropositive substituents in case of compounds **1**, **6**, **35**, **46** etc., and disfavor for electronegative substituents as in compounds **38**, **40**, **42**, **44**, **45** etc.

3.6.3. Hydrogen bond acceptor and donor contour analysis

Figs. 8 and 9 depict the hydrogen bond acceptor and donor contour maps of the CoMSIA models. Magenta contours encompass regions where a hydrogen bond acceptor will lead to improved biological activity, while an acceptor located near the red regions will result in impaired biological activity. Cyan color indicates the regions where hydrogen bond donor acts as favored and orange color refers to the disfavored regions. There are two big magenta

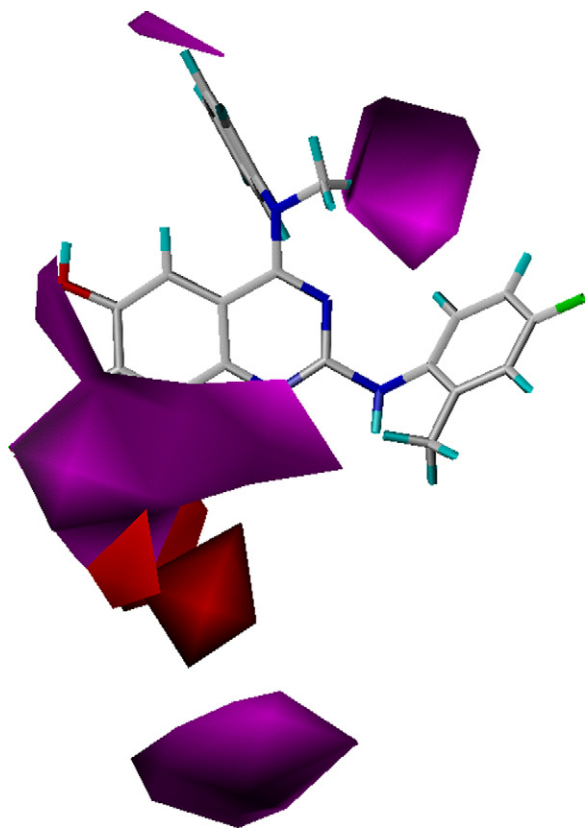


Fig. 8. CoMSIA contour maps illustrating acceptor features in combination with compound **163**. The magenta contour for H-bond acceptor group increase activity, red indicates the disfavored region.

contour maps in the Fig. 8, surrounding the R1 position of the heterocyclic ring, supports the requirement of H-bond acceptor. This can be seen in compounds **153**, **154**, **156** and **160–173**. The small red contours in the same figure, indicates that any hydrogen bond acceptors are not favored in these areas. This offers an explanation for the worse biological activity of compounds **8**, **12**, **83**, **95**, **109**, **130**, and **131** as their substituents having acceptor group at this position, are mapped to this region. There is another magenta contour exists in Fig. 8. Compounds with moderate to good hydrogen bond acceptor exactly fitted in this area and also shows good activity ranges. There are cyan contours in Fig. 9 supports the same opinion discussed above in Fig. 8. The presence of strong H-bond donor in compound **149** is responsible for its high activity. We can observe a good range of activity profile with most of the compounds with H-bond donors near these contours like in compounds **35**, **72**, **170**, **171**. The orange contours in this figure indicate that presence of strong H-bond donors is detrimental to the biological activity.

3.6.4. Hydrophobic contour analysis

Yellow and white contours enclose regions favorable for hydrophobic and hydrophilic groups respectively. The yellow contour map in Fig. 10 supports the importance of aromatic ring substitutions C² positions of heterocyclic ring as can be seen in scaffold C. This hydrophobic interaction might be very important for binding affinity, since this feature was also observed in CoMFA and CoMSIA steric contour maps. A small hydrophilic contour mapped very near to this C² position illustrating that unsubstituted amine group at this position is important for hydrogen bond interaction with the active site amino acids.

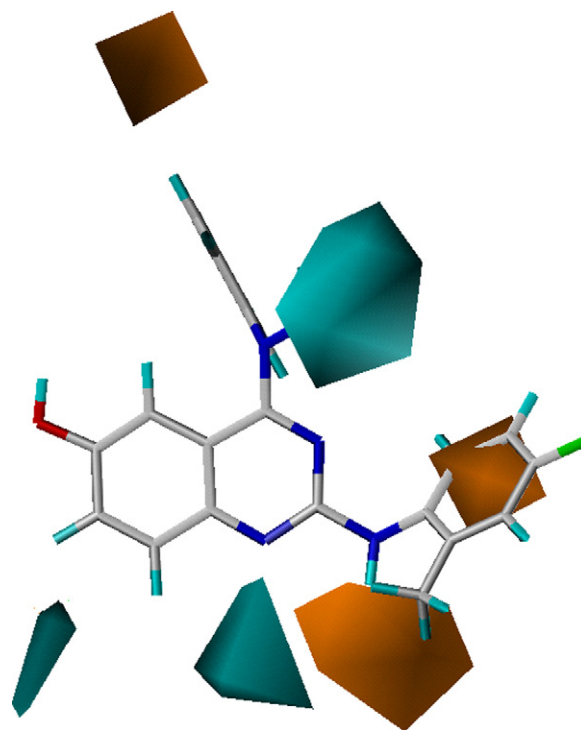


Fig. 9. CoMSIA contour maps illustrating donor features in combination with compound **163**. The cyan contour for H-bond donor favor region, orange indicates the disfavored region.

Nearly all the models performed well in the prediction of the activity of the test compounds with the best one being the CoMSIA model with all the descriptors having the highest r^2_{pred} of 0.917. In almost all cases, the predicted pIC₅₀ values are close to the observed values. Particularly, the above-mentioned model showed

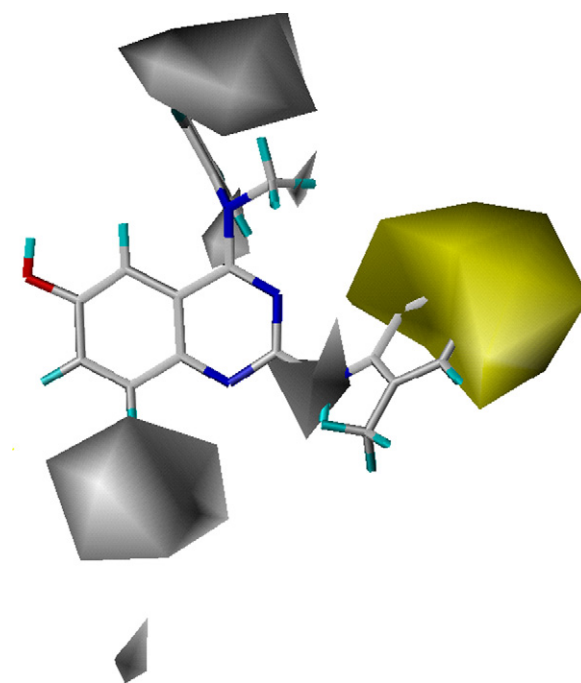


Fig. 10. CoMSIA contour maps illustrating hydrophobic features in combination with compound **163**. The yellow contour for hydrophobic favor region, white indicates the hydrophilic favored region.

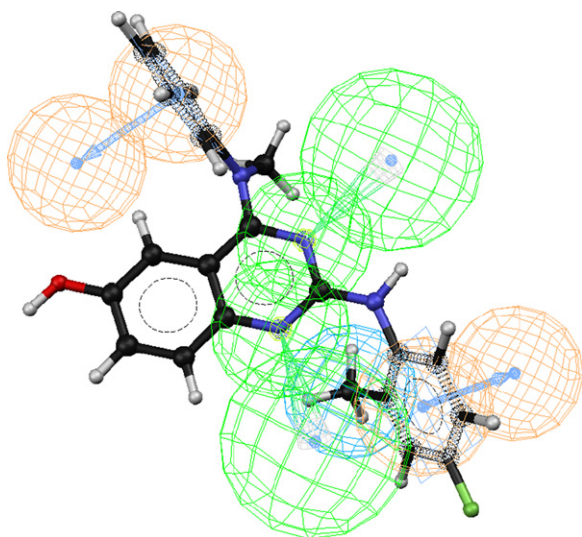


Fig. 11. Mapping of common featured pharmacophore model onto the compound **163**.

residuals no larger than 1 log unit. For the models containing only steric and electrostatic fields, r^2_{pred} for CoMFA is much higher than that for CoMSIA, also suggesting that CoMFA model is better than CoMSIA model with steric and electrostatic descriptors. Considering the flexibility of all the molecules and the lack of target information, the predictive qualities of the QSAR models are satisfying. Overall, based on r^2 , q^2 , and r^2_{pred} , the best model is CoMSIA model with all the five descriptors. This CoMSIA model, which includes steric, electrostatic, H-bond donor, H-bond acceptor, and hydrophobic fields, is the one we use for detailed analysis below, along with CoMFA model

3.7. Pharmacophore model

A qualitative pharmacophore model was generated to extract the common features among the highly active compounds using 23 compounds having activity >7.0 (pIC₅₀) with the help of Hip-Hop module of Catalyst software. The generated pharmacophore model which was mapped to the highest active compound **163** (having 'C' scaffold) was shown in the Fig. 11. The five-featured pharmacophore model contains two hydrogen bond acceptors, two ring aromatics and one hydrophobic feature. The two aromatic features are mapped to the two phenyl rings positioned at C² and C⁴ of quinazoline ring of the highest active compound **163**. Two hydrogen bond acceptors are mapped to the two electron rich nitrogen atoms of quinazoline ring and the hydrophobic group was mapped to the 2-methyl of the phenyl ring positioned at C² position. The pharmacophore model was also mapped to the highly active compounds **72** and **128** of scaffold A and B respectively (Figs. 1 and 2 supplementary information). Few of the features of pharmacophore model were not mapping to these compounds as they are not highly active when compared to compounds with 'C' scaffold. For compound **72**, acceptor and ring aromatic features are not mapping where as for compound **128** hydrophobic feature is missing.

4. Conclusion

Despite the lack of structural information on the gastric (H⁺/K⁺)-ATPase, the design of potent inhibitors has been attempted by means of comparative molecular field analysis and comparative

molecular similarity indices, a well-established 3D-QSAR techniques. In this study, 3D-QSAR models for structurally diverse quinoline, quinazoline analogues with statistical significance and predictive abilities by using CoMFA and CoMSIA methods were developed and validated. Good statistical parameters for CoMFA and CoMSIA indicate the existence of a similar relationship among all compounds used to build the model. In addition to steric and electrostatic fields, hydrophobic, H-bond acceptor and donor fields are also found to be important for inhibitory activities since the predictive power of the CoMSIA model appeared to be superior to that of CoMFA model. The significant predictive ability of 3D QSAR models observed for the external test set of 52 molecules makes these models useful for designing new compounds with good inhibitory properties against gastric (H⁺/K⁺)-ATPase.

Acknowledgement

We are thankful to the management of PGRRCD, Osmania University, Hyderabad for providing the software facility, Dr. J.A.R.P. Sarma, Director, Bioinformatics Division, GVK Biosciences Pvt. Ltd., and Dr. Soujanya, Scientist, IICT, Hyderabad for continuous support to carry out this work.

Appendix A. Supplementary data

Supplementary data associated with this article can be found, in the online version, at doi:10.1016/j.jmgm.2008.04.012.

References

- [1] W. Kuhlbrandt, Nat. Rev. Mol. Cell Biol. 5 (2004) 282–295.
- [2] J.A. Esplugues, Drugs 65 (2005) 7–12.
- [3] (a) R. Fass, M. Shapiro, R. Dekel, J. Sewell, Aliment Pharmacol. Ther. 22 (2005) 79–94; (b) N. Vakil, Aliment Pharmacol. Ther. 19 (2004) 1041–1049; (c) J. Tack, Curr. Opin. Gastroenterol. 21 (2005) 454–460.
- [4] W. Beil, I. Hackbarth, K.F. Sewing, Br. J. Pharmacol. 88 (1986) 19–23.
- [5] C. Briving, B.M. Andersson, P. Nordberg, B. Wallmark, Biochem. Biophys. Acta 946 (1988) 185–192.
- [6] B. Wallmark, C. Briving, J. Fryklund, K. Munson, R. Jackson, J. Mendlein, J. Biol. Chem. 262 (1987) 2077–2084.
- [7] D.J. Keeling, R.C. Malcolm, S.M. Laing, R.J. Iffe, C.A. Leach, Biochem. Pharmacol. 42 (1991) 123–130.
- [8] (a) K. Andersson, E. Carlsson, Pharmacol. Ther. 108 (2005) 294–307; (b) M.E. Parsons, D. Keeling, J. Expert Opin. Invest. Drugs 14 (2005) 411–421.
- [9] G.N. Tytgat, Aliment Pharmacol. Ther. 15 (2001) 6–9.
- [10] Herling, A.W., Weidmann, K., 5th ed., John Wiley, New Jersey, 1996.
- [11] J. Mossner, K. Caca, Eur. J. Clin. Invest. 35 (2005) 469–475.
- [12] W. Wurst, J. Yale, Biol. Med. 69 (1996) 233–243.
- [13] P.J. Chiu, C. Casciano, G. Tetzlo, J.F. Long, A. Barnett, J. Pharmacol. Exp. Ther. 226 (1983) 121–125.
- [14] A.L. Colin, H.B. Thomas, J.I. Robert, J.K. David, E.P. Michael, J.T. Colin, J.W. Kenneth, J. Med. Chem. 38 (1995) 2748–2762.
- [15] J.I. Robert, H.B. Thomas, B. Peter, J.K. David, A.L. Colin, L.M. Malcolm, E.P. Michael, J.T. Colin, J. Med. Chem. 38 (1995) 2763–2773.
- [16] T.I. Oprea, C.L. Waller, G.R. Marshall, J. Med. Chem. 37 (1994) 2206–2215.
- [17] Sybyl 6.7.1, Tripos Inc., 1699 South Hanley Road, St. Louis, Missouri, 63144, USA.
- [18] M. Clark, R.D. Cramer III, N.V. Opdenbosch, J. Comput. Chem. 10 (1989) 982–1012.
- [19] M.J.S. Dewar, E.G. Zoebisch, E.F. Healy, J.J.P. Stewart, J. Am. Chem. Soc. 107 (1985) 3902–3909.
- [20] Catalyst, version 4.6, Accelrys, Burlington, MA.
- [21] A. Smellie, S.L. Teig, P. Towbin, Poling: promoting codirectional coverage, J. Comput. Chem. 16 (1995) 171–187.
- [22] K. Kim, G. Greco, E. Novellino, Perspect. Drug Discov. Des. 12 (1998) 257–315.
- [23] R.D. Cramer, D.E. Patterson, J.D. Bunce, J. Am. Chem. Soc. 110 (1988) 5959–5967.
- [24] G. Klebe, U. Abraham, T. Mietzner, J. Med. Chem. 37 (1994) 4130–4136.
- [25] G. Klebe, U. Abraham, J. Comput. Aided Mol. Des. 13 (1999) 1–10.
- [26] S. Wold, C. Albano, W. Dunn, U. Edlund, K. Esbensen, P. Geladi, S. Hellberg, E. Johansson, W. Lindberg, M., Sjöström, in: K. Kowalski (Ed.), Reidel, Dordrecht, 1988, The Netherlands, pp. 17–95.
- [27] B.L. Bush, R.B. Nachbar, J. Comput. Aided. Mol. Des. 7 (1993) 587–619.